Motion Analysis of Pitch Rotation Mechanism for Posture Control of Butterfly-style Flapping Robot

Taro FUJIKAWA*[1], Masahiro SHINDO*[2] and Koki KIKUCHI*[3]
*1 Department of Robotics and Mechatronics, Tokyo Denki University
5 Senju Asahi-cho, Adachi-ku, Tokyo 120-8551, Japan
fujikawa@fr.dendai.ac.jp
*2,3 Department of Advanced Robotics, Chiba Institute of Technology
2-17-1 Tsudanuma, Narashino-shi, Chiba 275-0016, Japan
s1376014WE@s.chibakoudai.jp, kikut@ieee.org

Abstract
We developed a small flapping robot on the basis of movements made by a butterfly with a low flapping frequency of approximately 10 Hz, a few degrees of freedom of the wings, and a large flapping angle. In this study, we clarify the pitch rotation mechanism that is used to control its posture during takeoff for different initial pitch and flapping angles by the experiments of both manufactured robots and simulation models. The results indicate that the pitch angle can be controlled by altering the initial pitch angle at takeoff and the flapping angles. Furthermore, it is suggested that the initial pitch angle generates a proportional increase in the pitch angle during takeoff, and that certain flapping angles are conducive to increasing the tendency for pitch angle transition. Thus, it is shown that the direction of the flight led by periodic changing in the pitch angle can be controlled by optimizing control parameters such as initial pitch and flapping angles.
Keywords: butterfly, flapping robot, pitch angle, flapping angle, posture control

1 Introduction
Flying robots with various methods of lift and propulsion, such as unmanned air vehicles, airships, and multirotor helicopters, have been developed as observation systems because they are unaffected by ground conditions and have high versatility [1–3]. Although these robots exist in several sizes, smaller robots are effective for passing through narrow spaces. Here, flying creatures whose wings have high flight capabilities such as ability to turn at right angles and to accelerate at more than 10 G from takeoff. The flapping mechanism of small flying insects is particularly useful for maneuvering through narrow spaces, such as gaps between debris. Although many insect-scale flapping robots have been developed thus far, they have not achieved practical flight [4–8] because it is difficult to implement a heavy driving system such as a conventional actuator consisting of a motor, gears, and a battery in such a small body. In addition, the complexity of the link mechanism deteriorates the transmission efficiency because the viscosity factors such as friction are more dominant than inertia at this scale. To overcome such challenges, we developed a flapping robot modeled after a butterfly having a low flapping frequency of approximately 10 Hz and a few degrees of freedom (DOF) of the wings. This robot is equipped with a rubber motor as a lightweight actuator, which does not require converting electrical energy into mechanical energy. Furthermore, it contains a simple slider-crank mechanism with elastic links to enable a wide flapping angle. In our previous research [9–11], a manufactured flapping robot took off from an airspeed of 0 m/s and flew upward during the downstroke and then forward during the upstroke in a staircase pattern to mimic the flight trajectory of a butterfly. However, posture control was not realized. Here, one of the characteristics of the butterfly-style flight is a posture control mechanism that raises the body pitch angle during the downstroke and lowers it during the upstroke, thereby synchronizing with flapping motion. Although, a butterfly has a few DOF of the wings—control of its wings is complicated—this insect flies skillfully.

In this study, we analyze the periodical pitch rotation mechanism that affects the posture of a butterfly during the takeoff by using a manufactured flapping robot and numerical simulation. Furthermore, we clarify the posture control mechanism to realize autonomous flight of the flapping robot.

This paper is organized as follows: In section 2, we analyze the flight characteristics of a butterfly. In section 3, we describe the butterfly-style flapping robot and numerical simulation model. In section 4, we analyze and discuss the pitch rotation mechanism of both robots and the simulation models. Finally, in section 5, we conclude the paper and outline future works.

2 Flight characteristics of a butterfly
We analyzed the flight characteristics of a swallowtail butterfly (*Papilio xuthus*) during takeoff by using a 3-D high-speed camera system with a resolution of 640 × 480 pixels and 200 fps [10]. **Figure 1** shows the definitions of parameters used in the motion analysis, and **Fig. 2** displays stroboscopic images of a butterfly captured during takeoff. The red line in **Fig. 2** denotes the trajectory of the center of the thorax.

Figure 3 shows a typical example of the relationship between flapping and pitch angles. As shown in the figure, the downstroke of the flapping begins at approximately 80° and the upstroke begins at

approximately −60°; that is, a butterfly flaps its wings in asymmetric up-and-down motion. In addition, the pitch angle begins at approximately 20° and periodically changes with a phase difference of approximately 90° between the flapping and pitch angles. These results show that the asymmetric flapping angle and takeoff upon ascension affect the pitch rotation. It is thought that a butterfly controls its posture through effective management of these mechanisms.

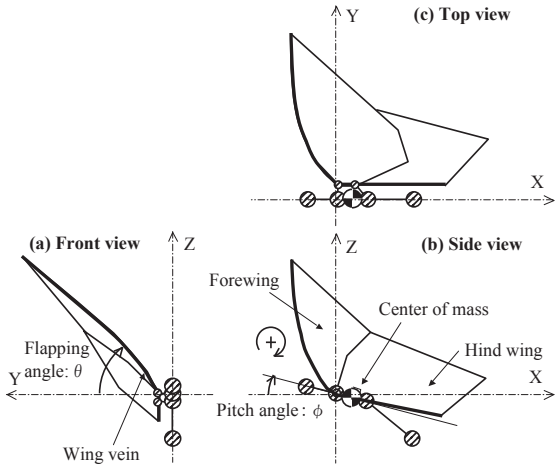

Fig. 1 Definitions of parameters used in motion analysis

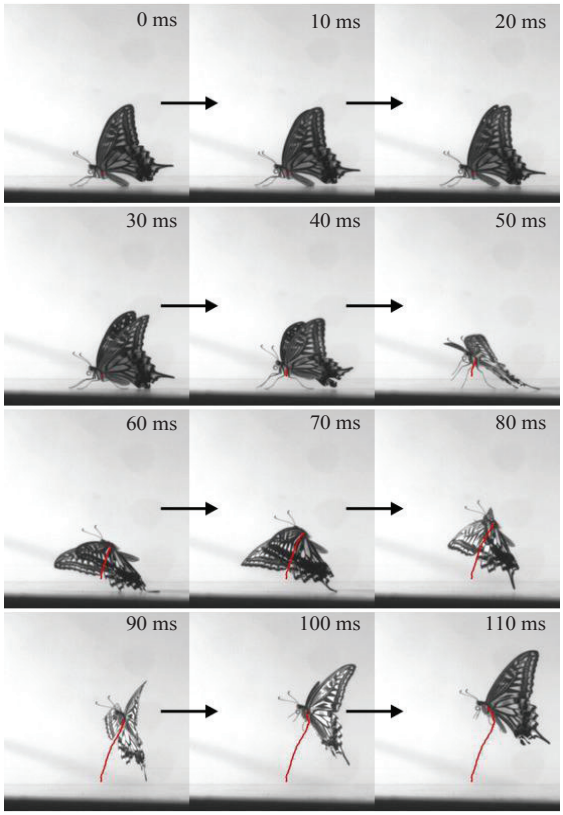

Fig. 2 Stroboscopic photographs of a butterfly captured during takeoff

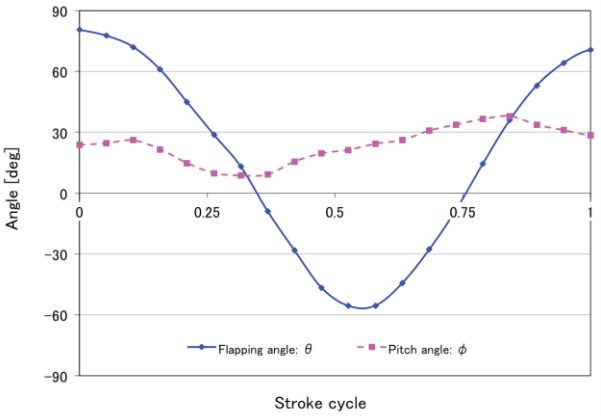

Fig. 3 Relationship between flapping and pitch angles during takeoff

3 Butterfly-style flapping robot and numerical simulation model

We manufactured a butterfly-style flapping robot and developed a numerical simulation model. The robot as shown in **Fig. 4**, which was constructed in bamboo to be lightweight, is equipped with a rubber motor as an actuator for a high power–mass ratio. The wing membranes are thin films made of polyethylene. The slider-crank mechanism mounted on its rear translates the rotation of the actuator into the flapping motion of the wings. By bending the elastic links, a wide flapping angle such as that from 80° to −60° is obtained compared with using rigid links (see ref. [10] for details).

Figure 5 shows the simulation model, the body of which consists of four mass points including the head, thorax 1, thorax 2, and abdomen, which are connected by springs and dampers. Both right and left wings are integrated with the respective fore and hind wings for synchronous movement. Each wing is divided in Nx-1 points along the wingspan direction and in Ny-1 points along chord direction, which are connected by springs and dampers. The finite element method (FEM) was used to calculate the body and wing motions and flow field around the wings; details have been previously documented [11].

The manufactured robot was used in takeoff experiments to observe trajectories of the flight and transitions of its pitch angle. To analyze its lift, thrust, and pitch rotation moment around the center of mass, we used numerical simulation.

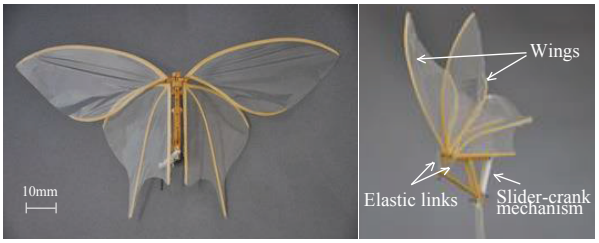

Fig. 4 Butterfly-style flapping robot

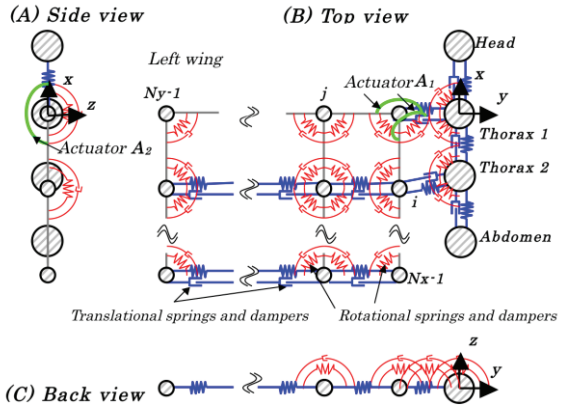

Fig. 5 Numerical simulation model

4 Motion analysis of pitch rotation mechanism

4.1 Parameters of flapping robots

To analyze the flight characteristics for the pitch rotation mechanism, we manufactured three models. Model A has a flapping angle of 80° to −60°, and an initial pitch angle of 15° based on the results of analysis of a butterfly. Model B has the same flapping angle as that of Model A; however, its initial pitch angle is 0°. Model C has a flapping angle of 60° to −80° and an initial pitch angle of 15°. The wing length and the chord length of each model are 53 mm and 42 mm, respectively, and the total mass of each model, including an actuator, is approximately 520 mg, which is equivalent to that of a butterfly.

We then performed experiments to clarify the following relationships for the takeoff motion by using a flapping frequency of 12 Hz for each model:

(1) For different initial pitch angles, a comparison experiment was conducted by using Model A and Model B.

(2) For different flapping angles, a comparison experiment was conducted by using Model A and Model C.

Table 1 shows these experimental parameters.

Table 1 Parameters of flapping robots

	Model A	Model B	Model C
Flapping angle [deg]	80〜-60	80〜-60	60〜-80
Initial pitch angle [deg]	15	0	15
Flapping frequency [Hz]	12	12	12

4.2 Settings of numerical simulation models

The structural parameters of the numerical simulation models corresponded to those of manufactured flapping robot, including a wing length of 53 mm, chord length of 42 mm, body length of 38 mm (head 4 mm, thorax 10 mm, abdomen 24 mm), total mass of 520 mg (head 60 mg, thorax 150 mg, abdomen 210 mg, wing 100 mg), and wing thickness of a uniform 0.3 mm.

The computational scheme included the following parameters: wings were divided into Nx = 16 along the wingspan direction and Ny = 12 along the chord direction; node number of FEM was approximately 700,000. The computational space was set to be approximately 1,300 × 1,000 × 1,000 mm.

4.3 Results and discussion

4.3.1 Different initial pitch angles

Figures 6 and **7** show stroboscopic photographs of takeoff of models A and B, respectively, which were captured by a high-speed camera. **Figures 8** and **9** show comparisons of transitions of pitch angle and trajectories of center mass. **Figures 10, 11**, and **12** show comparisons of transitions of lift, thrust, and pitch rotation moment, respectively, of models A and B by numerical simulation.

The experiments revealed that the transition of pitch angle increased at a rate proportional to the initial pitch angle (**Fig. 8**). An increase in initial pitch angle to Model A resulted in stronger backward flight during the downstroke than that observed in Model B (**Fig. 9**). The maximum lifts of models A and B were 0.028 N and 0.029 N, respectively, and maximum thrusts were 0.011 N and 0.012 N, respectively, for backward direction during the downstroke. Because the pitch angle at the beginning of the upstroke of Model A (42°) became larger than that of Model B (29°), the lift of Model A (−0.024 N) increased over that of Model B (−0.021 N). That is, the flight level was lower in Model B (**Fig. 10**), and the thrust of Model A at 0.025 N was larger than that of Model B at 0.023 N for foreword direction at a stroke cycle of approximately 0.75 (**Fig. 1**1). However, as shown **Fig 12**, the transitions of the pitch rotation moment showed little differences between the models because the angles of the downstrokes and upstrokes of both models were equal.

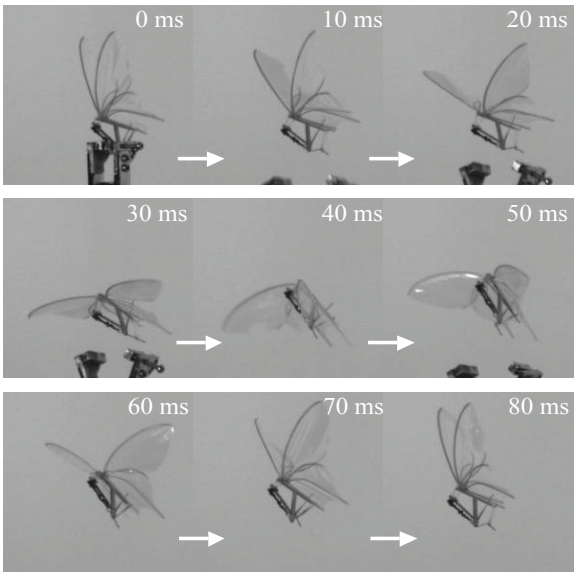

Fig. 6 Stroboscopic photographs of Model A captured during takeoff

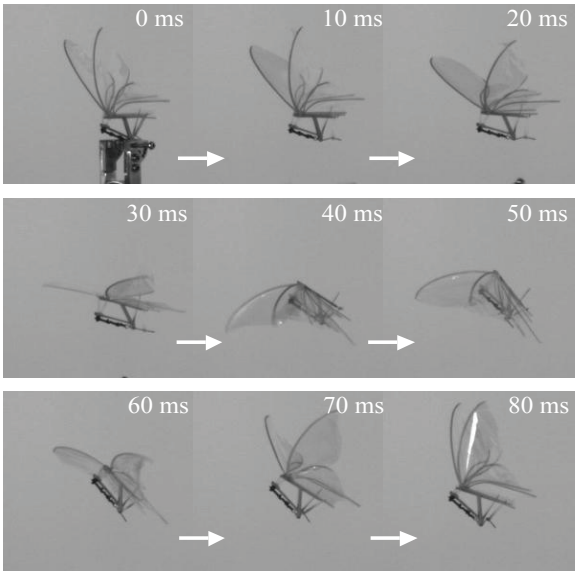

Fig. 7 Stroboscopic photographs of Model B captured during takeoff

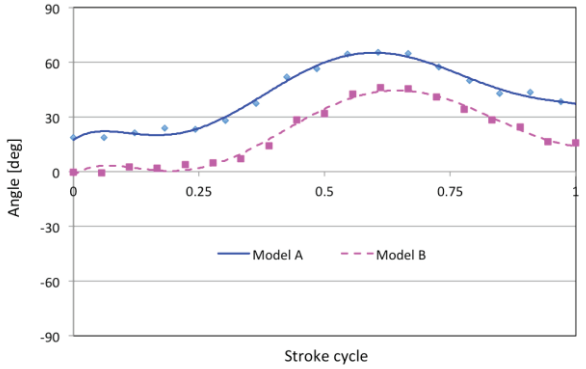

Fig. 8 Transitions of pitch angles of models A and B for manufactured flapping robot

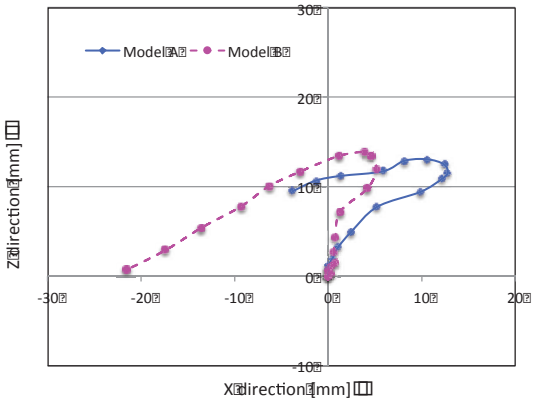

Fig. 9 Trajectories of center of mass during takeoff of models A and B for manufactured flapping robot

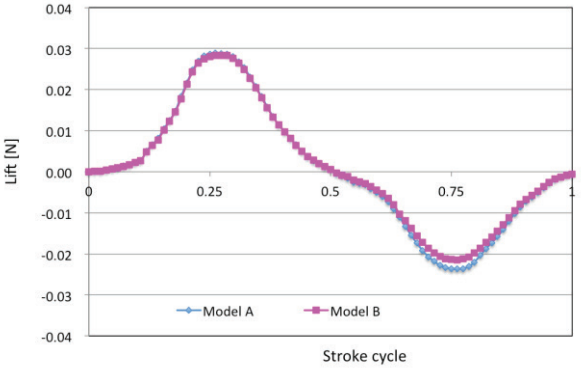

Fig. 10 Transitions of lift of models A and B by numerical simulation

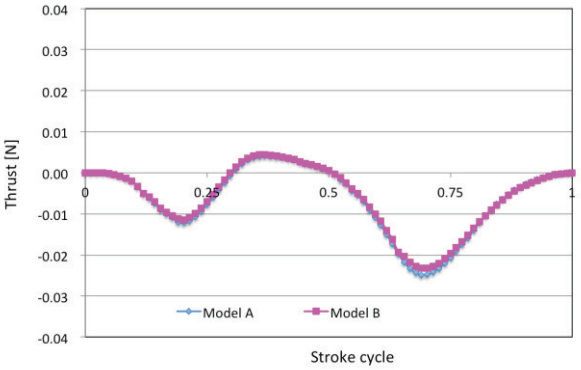

Fig. 11 Transitions of thrust of models A and B by numerical simulation

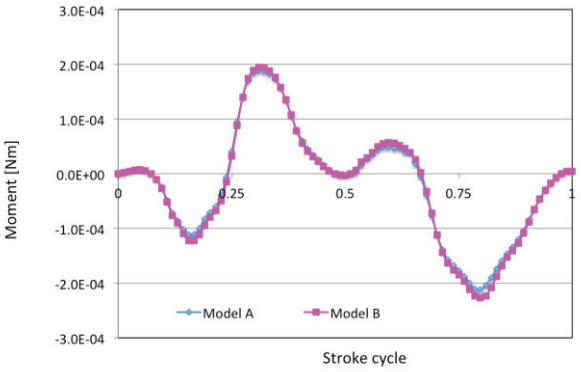

Fig. 12 Transitions of pitch moment of models A and B by numerical simulation

4.3.2 Different flapping angles

We performed the same experiments to compare different flapping angles during takeoff. **Figure 13** shows stroboscopic photographs captured during takeoff of Model C. **Figures 14** and **15** show comparisons of transitions of pitch angle and trajectories of center mass of manufactured hardware. **Figures 16, 17**, and **18** show comparisons of transitions of lift, thrust, and pitch rotation moment of simulation models, respectively.

The transition of pitch angle of Model C showed an increasing tendency compared to that of Model A (**Fig. 14**). Therefore, Model C showed stronger backward movement during the downstroke and more

upward movement during the upstroke (**Fig. 15**). Moreover, the lift during the downstroke of Model C reached a maximum faster than that of Model A, and its value at 0.031 N was larger than that of Model A. During the upstroke, distinctive characteristics of the transitions of lift were noted. The lift of Model C reached a maximum faster than that of Model A; however, although the lift of Model A was always negative, that of Model C remained positive until approximately 0.75 strokes (**Fig. 16**). This result occurred because the pitch angle at the beginning of the upstroke was more than 60°, and the direction of the reaction force of the wings became downward. Therefore, the force of the flapping during the upstroke generated the lift. Here the maximum lift of Model C was 0.005 N. For thrust during the downstroke, because the pitch angle of Model C became larger than that of Model A, the thrust of Model C shifted to positive at an earlier point, which was observed as backward flight, than that of Model A (**Fig. 17**). During upstroke, because the pitch angle of Model C reached nearly 90°, its thrust was larger than that of Model A. The maximum thrusts of Model C during downstroke and upstroke were 0.007 N and 0.030 N, respectively. As shown in **Fig 18**, because the total pitch rotation moment of Model C was larger than that of Model A, its nose-up movement was also larger than that of Model A. Hence, the pitch angle of Model C was increased over that of Model A. However, if the pitch angle at the start of the second stroke becomes over 45 deg, reaction force of the wings during downstroke generates backward thrust and then hardware does a backflip. Therefore, it is necessary to control the body pitch angle over 45 deg at the end of downstroke and under 45 deg at the end of upstroke like a Model A in the case of level flight.

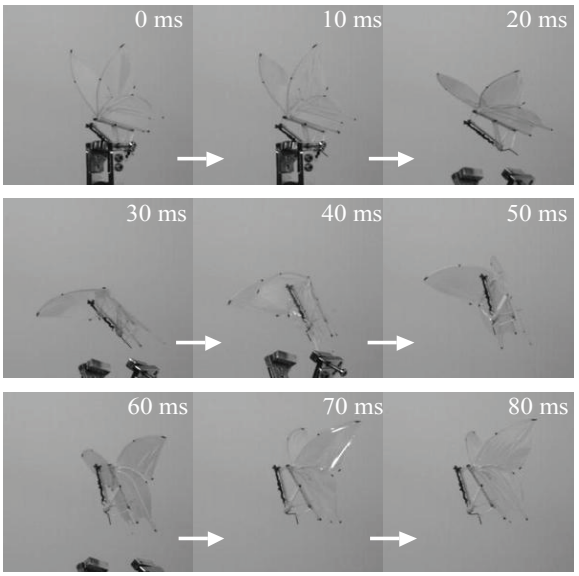

Fig. 13 Stroboscopic photographs of Model C captured during takeoff

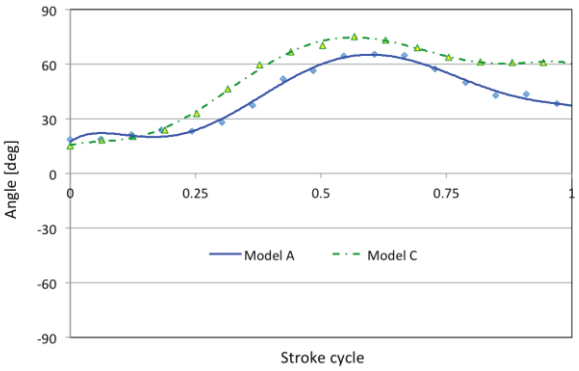

Fig. 14 Transitions of pitch angle of models A and C for manufactured flapping robot

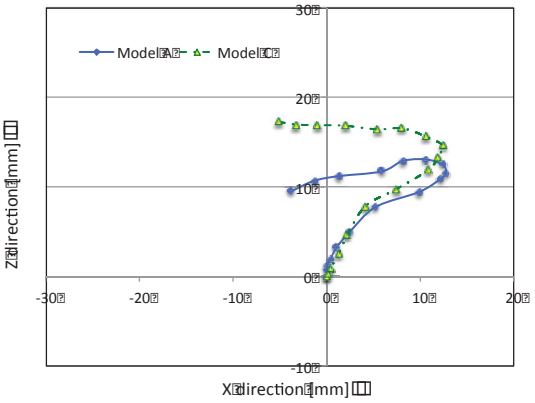

Fig. 15 Trajectories of center of mass during takeoff of models A and C for manufactured flapping robot

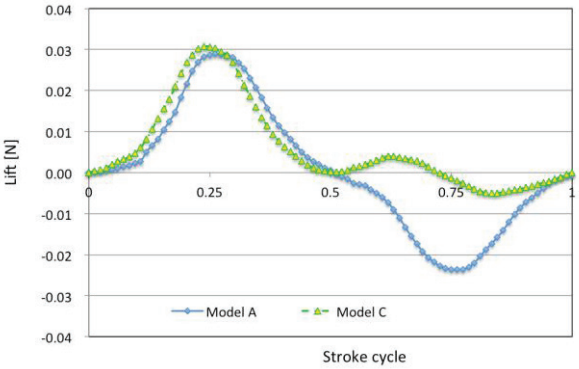

Fig. 16 Transitions of lift of models A and C

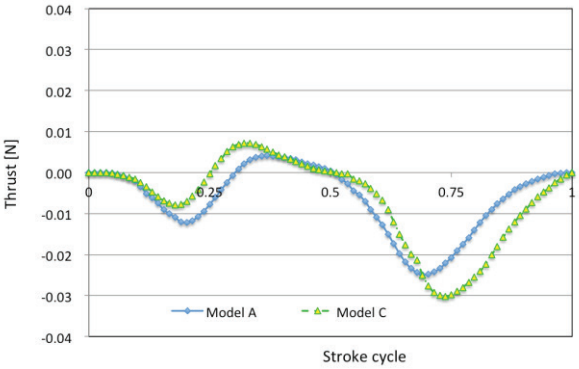

Fig. 17 Transitions of thrust of models A and C

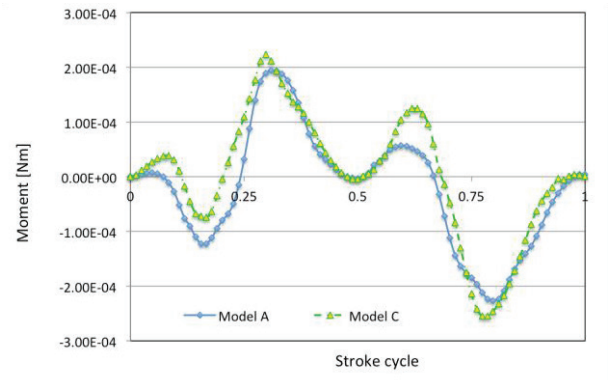

Fig. 18 Transitions of pitch moment of models A and C by numerical simulation

5 Conclusions

To realize posture control of a butterfly-style flapping robot, we analyzed the pitch rotation mechanism that occurs during takeoff by performing experiments of hardware and numerical simulation for different initial pitch angles and flapping angles.

We demonstrated that the pitch angle is controlled by the initial flapping angle at takeoff for increasing the angle and by different flapping angles to generate the increasing tendency in the transition of the pitch angle. Thus, it was shown that these parameters control the direction of flight.

In future research, we aim to investigate the mechanism for yaw and roll control to realize autonomous flight of a butterfly-style flapping robot.

Acknowledgements

This research was partially supported by Research Institute for Science and Technology of Tokyo Denki University Grant Number Q13T-06/Japan. The authors would like to express their deep gratitude to all involved in the research project.

References

[1] E. W. Green and P. Y. Oh, Autonomous "Hovering of a Fixed-Wing Micro Air Vehicle", *Proceedings of 2006 IEEE International Conference on Robotics and Automation*, (2006), pp. 2164-2169.

[2] T. Fukao, K. Fujitani, T. Kanade, "An autonomous blimp for a surveillance system", *Proceedings of 2003 IEEE/RSJ International Conference on Intelligent Robots and Systems (IROS)*, (2003), pp. 1829-1825.

[3] G. Hoffman, H. Huang, *et al.*, "Quadrotor Helicopter Flight Dynamics and Control: Theory and Experiment", *Proceedings of 2007 International Conference on the American Institute of Aeronautics and Astronautics*, (2007), pp. 1-20.

[4] X. Deng, L. Schenato, W. Chung Wu, and S. S. Sastry, "Flapping Flight for Biomimetic Robotic Insects: Part I – System Modeling," *IEEE Trans. Rob.*, Vol. 22, No. 4, (2006), pp. 776-788.

[5] R. S. Fearing, K. H. Chiang, M. H. Dickinson, D. L. Pick, M. Sitti, and J. Yan, "Wing Transmission for a Micromechanical Flying Insect," *proceedings of IEEE International Conference on Robotics and Automation*, (2000), pp. 1509-1516.

[6] M. Sitti, "PZT Actuated Four-Bar Mechanism with Two Flexible Links for Micromechanical Flying Insect Thorax," *proceedings of IEEE International Conference on Robotics and Automation*, (2001), pp. 3893-3900.

[7] R. J. Wood, "The First Takeoff of a Biologically Inspired At-Scale Robotic Insect," *IEEE Trans. Rob.*, Vol. 24, No. 2, (2008), pp. 341-347.

[8] R. J. Wood, "Design, fabrication, and analysis of a 3 DOF, 3cm flapping-wing MAV," *proceedings of IEEE International Conference on Intelligent Robots and Systems*, (2007), pp. 1576-1581.

[9] T. Udagawa, T. Fujikawa, X. GAO, and K. Kikuchi, "Development of a Small-Sized Flapping Robot", JSDE The 1st International Conference on Design Engineering and Science, (2005), pp.283-288.

[10] T. Fujikawa, Y. Sato, T. Yamashita, and K. Kikuchi, "Development of A Lead-Lag Mechanism Using Simple Flexible Links for A Small Butterfly-Style Flapping Robot", ISIAC2010, (2010).

[11] T. Fujikawa, *et al.*, "Development of a Small Flapping Robot -Motion Analysis during Takeoff by Numerical Simulation and Experiment-", Mechanical Systems and Signal Processing (MSSP), Vol.22, No.6, (2008), pp.1304-1315.

Received on November 30, 2013
Accepted on February 20, 2014